PCCP

Accepted Manuscript

This article can be cited before page numbers have been issued, to do this please use: U. Kuenzer, J. Soraru and T. Hofer, *Phys. Chem. Chem. Phys.*, 2016, DOI: 10.1039/C6CP06698D.

ROYAL SOCIETY OF CHEMISTRY

www.rsc.org/pccp

View Article Online
DOI: 10.1039/C6CP06698D

Pushing the limit for the grid-based treatment of Schroedinger's equation: a sparse Numerov approach for one, two and three dimensional quantum problems

*Ulrich Kuenzer, Jan-Andrè Sorarù and Thomas S. Hofer**

Theoretical Chemistry Division

Institute of General, Inorganic and Theoretical Chemistry

Center for Chemistry and Biomedicine

University of Innsbruck, Innrain 80-82, A-6020 Innsbruck, Austria

E-Mail: T.Hofer@uibk.ac.at

Tel.: +43-512-507-57111

Fax: +43-512-507-57199

September 29, 2016

*Corresponding author

View Article Online
DOI: 10.1039/C6CP06698D

Abstract

The general Numerov method employed to numerically solve ordinary differential equations of second order was adapated with special focus to solving Schrödinges equation. By formulating a hierarchy of novel stencil expressions for the numerical treatment of the Laplace operator in one, two and three dimensions the method could not only be simplified over the standard Numerov scheme. The improved framework enables the natural use of matrix sparsity to reduce the memory demand and the associated computing time, thus enabling the application of the method to larger problems.

The performance of the adapted method is demonstrated using exemplary harmonic and Morse problems in one and two dimensions. Furthermore, the vibrational frequencies of molecular hydrogen and water are calculated, inherently considering the influence of anharmonicity, mode-mode coupling and nuclear quantum effects. The estimation of the tunneling splitting in malonaldehyde serves as an example for a two-dimensional problem.

1 Introduction

The general form of the time-independent one dimensional Schrödinger equation is given as

$$-\frac{\hbar^2}{2m}\Delta\psi(x) + V(x)\psi(x) = E\psi(x), \tag{1}$$

with the Laplace operator Δ, the potential V, the energy E, the (reduced) mass m and the wavefunction ψ [1]. $\hbar$ denotes the reduced Planck constant. Only in a few simple cases the Schrödinger equation can be solved analytically, but a large number of approaches to solve this equation numerically have been formulated. The resulting energy levels and wavefunctions are required to describe various physical and chemical phenomena, as for instance the vibrational spectra of molecules [2,3]. The wavefunctions can then be used to calculate different properties of chemical systems, *e.g.* the coupling strength of different vibrations [4, 5] or their respective spectral intensities.

In addition to the application in the spectroscopy such methods enable investigations the behaviour of particles in different potentials. This investigations can help to obtain a deeper understanding of

View Article Online
DOI: 10.1039/C6CP06698D

the interactions between particles and potentials, e.g. the behaviour of an electron in the electric field of a scanning tunneling microscope or a hydrogen atom in a chemical reaction.

Among the various different approaches a family of numerical frameworks use grid-based methods to solve the Schrödinger equation (1). They can be divided into shooting methods [6] and the more advanced matrix methods [7]. Shooting methods calculate ψ at a particular gridpoint based on the information of the previous ones, typically applying adequate boundary conditions. A shortcoming of this methods is that a reliable initial guess is required to find a particular solution within few iterations. The matrix methods turn (1) into a matrix eigenvalue equation. The eigenvalues are the energy levels and the eigenvectors represent the wavefunctions at the gridpoints.

All grid based methods approximate the Hamiltonian in different ways. These approximations lead to a matrix eigenvalue equation which can be solved with comperatively simple algebraic methods, with the advantage that all states can be calculated at once from diagonalisation of the matrix. In general this methods are only limited by the matrix size and the time needed to calculate the eigenvalues and eigenvectors. The larger the grids get the more memory and computational time is needed.

The method differ in the way the Hamiltonian, in particular the Laplace operator, is approximated. One of the most widely used grid-based methods is the Numerov approach [8, 9]. Here the second derivation is approximated using finite differences on an equispaced grid [10]. In [2, 11–13] the adequate performance of the Numerov method is demonstrated leading to reasonable results already with comperatively small grids. In [14] it was shown that the accuracy of Numerv's method can be raised using a bigger stencil.

A similar method to solve the Schrödinger equation (1) is the Chebyshev collocation approach [15, 16]. In this method the gridpoints are placed at the roots of the chebychev polynomials and therefore, are not equally spaced. If the number of gridpoints is increased, all gridpoints have to be evaluated again, which is a potential shortcoming of this framework. Using equispaced grids in the Numerov formulation only the missing gridpoints have to be evaluated. In [11] it was shown that the results are slightly better than the results of the standard Numerov method.

A third commonly used method also based on the use of equispaced grids is the discrete variable rep-

View Article Online
DOI: 10.1039/C6CP06698D

resentation (DVR) [17,18], here the Hamiltonian is approximated by representing the wavefunctions via *sinc*() basis-functions. This approach leads to accurate estimations of energies and eigenvalues already on small grids [11]. If, howewer, in addition to the energy levels the wavefunctions with a tight spacing are required, the DVR approach suffers from a significant computational overhead.

In [11] all three methods were extended to two and three dimensions in order to investigate the quantum mechanical properties of hydrogen atoms in an organic molecule. It was shown that the Chebyshev method and the DVR method outperform the standard Numerov method regarding the accuracy on small grids.

Calculating the energies and wavefunctions of a system, the wavefunctions are only known at the grid points. If the wavefunctions are used to investigate properties of a quantum system it can often be required to work with more tightly spaced grids. This provides a better approximation for the wavefunctions and therefore more accurate results especially in case of excited states. To compensate the increased gridsize a method with a comparably smaller computational effort is highly desirable.

Using specialized numerical methods the effort in computing eigenvalues and eigenvectors is dramatically reduced if the associated matrices are sparse (*i.e.* contain a large number of zero entries). In this paper a modified Numerov-type method in one, two and three dimensions is presented, allowing to choose the desired accuracy of the approximation. Energies and wavefunctions are calculated using suitable algorithms taking advantage of matrix sparsity. The higher the dimension, the sparser the matrix gets, reducing the required memory and CPU capacities significantly. The new approach also simplifies the Numerov procedure, while at the same time ensuring that the associated matrices are symmetric, thus guaranteeing real eigenvalues and orthogonality of the wavefunctions.

View Article Online
DOI: 10.1039/C6CP06698D

2 Methods

2.1 Improved Numerov Method

Numerov's method can be applied to all ordinary differential equations of the form

$$\Delta\psi(\mathbf{x}) = f(\mathbf{x})\psi(\mathbf{x}), \tag{2}$$

with the Laplace operator Δ, the discretized vector $\mathbf{x}$ and a known function f. The function $\psi(\mathbf{x})$ is unknown. Rearrangement of Schrödingers equation leads to a form compatible with the Numerov framework:

$$\Delta\psi(\mathbf{x}) = \frac{2m}{\hbar^2}\Big(V(\mathbf{x}) - E\Big)\psi(\mathbf{x}) = f(\mathbf{x})\psi(\mathbf{x}) \tag{3}$$

with the potential $V(\mathbf{x})$ and the energy eigenvalue E. It has been shown that using Numerov's method [7] energy eigenvalues and wavefunctions of a given quantum system can be written in form of

$$\mathbb{A}\psi + \mathbb{B}\mathbb{V}\psi = E\mathbb{B}\psi. \tag{4}$$

Rearrangement yields the matrix eigenvalue equation

$$(\mathbb{B}^{-1}\mathbb{A} + \mathbb{V})\psi = E\psi, \tag{5}$$

with eigenvalue E and eigenvector ψ.

In one dimension the matrices $\mathbb{A}$ and $\mathbb{B}$ are tridiagonal matrices [7]. In higher dimensions the composition of the matrices turns into blockwise filled matrices [11], but the problem still comprises an eigenvalue equation. The exact form of the matrices are discussed in the following sections. In all dimensions the matrices $\mathbb{A}$ and $\mathbb{B}$ are sparse filled, with increasing sparsity as the matrix size is increased.

In respective of the dimension Numerov's approach is linked to two main disadvantages:

1. The accuracy of the standard Numerov method is limited to $\mathcal{O}(h^4)$, h representing the distance

View Article Online
DOI: 10.1039/C6CP06698D

between two gridpoints.

2. $\mathbb{A}$ and $\mathbb{B}$ are sparse filled, symmetric matrices. However, the product $\mathbb{B}^{-1}\mathbb{A}$ in equation (5) is in general neither symmetric nor tridiagonal or sparse.

Tang proposed an approach to raise the accuracy of Numerov's method in one dimension to arbitrary order [14]. Higher accuracy is achieved by regarding more gridpoints for the approximation of the second derivative in the Hamiltonian. To reach the accuracy $\mathcal{O}(h^{2n})$ in the one-dimensional case $2n+1$ gridpoints have to be included in the respective stencil. The resulting matrices have more entries close to the diagonal but the sparse character of the matrices $\mathbb{A}$ and $\mathbb{B}$ remains conserved. However, as mentioned the resulting matrix $\mathbb{B}^{-1}\mathbb{A}$ is in general not sparse and not symmetric. A symmetric matrix has only real eigenvalues and the eigenfunctions are orthogonal to each other, crucial prerequisites for the energy levels and wavefunctions of quantum mechanical systems. Thus, using a symmetric matrix in the eigenvalue problem ensures these properties in the solution.
In this article both problems are adressed, while raising the accuracy of the method using higher stencils. Simultaneously a sparse filled, symmetric matrix is derived in one, two and three dimensions in order to make use of the advantages discussed above. The derivation of the three-dimensional case is included in the supplementary material. In addition the use of the sparse character in the actual implementations leads to a significantly lowered memory demand and greatly reduced execution times.

2.1.1 One Dimension

Before the standard Numerov method is outlined and the modified method is derived, the notation has to be clarified. A grid of N points x_i with $i = 1, \ldots, N$ is investigated, following the short notation

$$\psi(x_i) = \psi_i \text{ and } \psi(x_i \pm k \cdot h) = \psi_{i\pm k},$$

where k denotes a natural number and all ψ_i with $i < 1$ and $i > N$ are considered zero, implying a zero (Dirichlet) boundary condition.
In one dimension the Laplace operator Δ becomes the second derivative $\partial^2/\partial x^2$. Replacing the

View Article Online
DOI: 10.1039/C6CP06698D

second derivative with a numerical expression yields

$$\psi_{i+1} - 2\psi_i + \psi_{i-1} = h^2 f_i \psi_i + 2\sum_{k=2}^{n} \frac{h^{2k}}{(2k)!}\psi_i^{(2k)} + \mathcal{O}(h^{2n+2}). \tag{6}$$

In the standard approach the sum is truncated at $n = 2$:

$$\psi_{i+1} - 2\psi_i + \psi_{i-1} = h^2 f_i \psi_i + 2\frac{h^4}{4!}\psi_i^{(4)} + \mathcal{O}(h^6). \tag{7}$$

Using the identity $\frac{\partial^4 \psi}{\partial x^4} = \frac{\partial^2 f\psi}{\partial x^2}$ in combination with $\psi_i'' = (\psi_{i+1} - 2\psi_i + \psi_{i-1})/h^2 + \mathcal{O}(h^2)$ leads after the division by h^2 to the main equation of the standard Numerov method:

$$\frac{1\psi_{i+1} - 2\psi_i + 1\psi_{i-1}}{h^2} = \frac{1}{12}\left(1f_{i+1}\psi_{i+1} + 10f_i\psi_i + 1f_{i-1}\psi_{i-1}\right) + \mathcal{O}(h^4). \tag{8}$$

Note, that due to this division by h^2 the order of the approximation is reduced to $\mathcal{O}(h^4)$. Summarizing this formula for all points ψ_i yields the respective matrix formulation

$$\mathbb{A}\psi = \mathbb{B}f\psi, \tag{9}$$

with stencils for the matrices $\mathbb{A}$ and $\mathbb{B}$ being $\frac{1}{h^2}(1, -2, 1)$ and $\frac{1}{12}(1, 10, 1)$, f is the function given in formula (2). Typically the values f_i are included in the matrix $\mathbb{B}$. Reinserting f as given in (3) and splitting of $\mathbb{V}$ and E leads to

$$\mathbb{A}\psi + \mathbb{B}\mathbb{V}\psi = E\mathbb{B}\psi.$$

Both matrices $\mathbb{A}$ and $\mathbb{B}$ are tridiagonal, the diagonal matrix $\mathbb{V}$ represents the potential at the gridpoints. In [14] an approach was discussed to raise the accuracy of the method by choosing a higher n. The bigger stencils were shown to raise the accuracy but don't change the form of the matrices, being filled only close to the diagonal.

Related approaches, like the Chebyshev collocation method or the discrete variable representation in one dimension lead on the other hand to a completely filled and thus dense matrix, which despite the inherently higher accuracy might prove disadvantageous. For this reason the development of a

View Article Online
DOI: 10.1039/C6CP06698D

more accurate Numerov method preserving a sparse matrix is crucial in case of larger grids as well as higher dimensions.

With this aim an adapted Numerov method was developed. After choosing the desired accuracy n in equation (6) the derivatives have to be approximated using the respective finite difference expressions. An approach with the accuracy $\mathcal{O}(h^6)$ is derived exemplarily in the following. Other levels of accuracy can be derived analogously.

$$f_i\psi_i = \frac{\psi_{i+1} - 2\psi_i + \psi_{i-1}}{h^2} - 2\frac{h^2}{4!}\psi_i^{(4)} - 2\frac{h^4}{6!}\psi_i^{(6)} + \mathcal{O}(h^6). \tag{10}$$

Approximating the fourth derivative using finite differences with an accuracy of $\mathcal{O}(h^4)$ and the sixth derivative with an accuracy of $\mathcal{O}(h^2)$ leads to

$$f_i\psi_i = \frac{1}{h^2}\left(\frac{1}{90}\psi_{i+3} - \frac{3}{20}\psi_{i+2} + \frac{3}{2}\psi_{i+1} - \frac{49}{18}\psi_i + \frac{3}{2}\psi_{i-1} - \frac{3}{20}\psi_{i-2} + \frac{1}{90}\psi_{i-3}\right) + \mathcal{O}(h^6). \tag{11}$$

It is important that all terms lead to the same $\mathcal{O}$ notation to reach the full accuracy. As one can easily see in this approach the left side of equation (11), the former $\mathbb{B}$ matrix, in this case is an identity matrix and can thus be neglected. The right side, representing the $\mathbb{A}$ matrix is a symmetric matrix with entries only close to the diagonal. Using this stencil equation (9) simplifies to

$$\mathbb{A}\psi = f\psi. \tag{12}$$

For the application to the Schrödinger equation this leads to the matrix eigenvalue equation

$$(\mathbb{A} + \mathbb{V})\psi = \mathbb{H}\psi = E\psi. \tag{13}$$

Since the potential matrix $\mathbb{V}$ is a diagonal matrix, the matrix $\mathbb{H}$ is sparse filled and symmetric. For instance the resulting matrix of a grid with 100 points is filled to 7%, a 1000 point grid leads to a matrix where only 0.7% of the entries are filled. Especially in higher dimensions this sparsity property of the matrix is of particular advantage. The respective algorithms are discussed in section

View Article Online
DOI: 10.1039/C6CP06698D

2.3.

2.1.2 Two Dimensions

In two dimensions the differential equation

$$\left(\frac{\partial^2}{\partial x^2}+\frac{\partial^2}{\partial y^2}\right)\psi(x,y)=f(x,y)\psi(x,y) \tag{14}$$

has to be solved on an $N \times M$ grid. In both dimensions the spacing h of the grid has to be the same. Analogously to the one dimensional case a shortened notation is used:

$$\psi(x_i,y_j)=\psi_{i,j} \text{ and } \psi(x_i \pm k\cdot h, y_j \pm l\cdot h)=\psi_{i\pm k,j\pm l}.$$

Additionally, a new notation is introduced where the $\psi_{i,j}$ terms are removed and only its coefficients are mentioned. The coefficients in the following are given in the same order as the $\psi_{i,j}$ are arranged below:

$$\begin{pmatrix} \psi_{i+1,j-1} & \psi_{i+1,j} & \psi_{i+1,j+1} \\ \psi_{i,j-1} & \psi_{i,j} & \psi_{i,j+1} \\ \psi_{i-1,j-1} & \psi_{i-1,j} & \psi_{i-1,j+1} \end{pmatrix}. \tag{15}$$

As in the one dimensional case the derivation starts with a sum of four individual Taylor-series:

$$\psi_{i+1,j+1}+\psi_{i+1,j-1}+\psi_{i-1,j+1}+\psi_{i-1,j-1}-4\psi_{i,j}=2h^2 f_{i,j}\psi_{i,j}+4\sum_{k=2}^{n}\frac{h^{2k}}{(2k)!}\left(\sum_{l=0}^{k}\frac{(2k!)}{(2k-2l)!2l!}\frac{\partial^{(2k)}\psi}{\partial x^{2k-2l}\partial y^{2l}}\right)+\mathcal{O}(h^{2n+2}) \tag{16}$$

choosing $n=2$ leads to the standard Numerov method in two dimensions [11]. The fourth derivatives are approximated by

$$\left(\frac{\partial^4\psi}{\partial x^4}+2\frac{\partial^4\psi}{\partial x^2\partial y^2}+\frac{\partial^4\psi}{\partial y^4}\right)=\frac{\partial^2(f\psi)}{\partial x^2}+\frac{\partial^2(f\psi)}{\partial y^2},$$

View Article Online
DOI: 10.1039/C6CP06698D

where the second derivatives are approximated using finite differences. The missing derivative is approximated by

$$h^4 \frac{\partial^4 \psi}{\partial x^2 \partial y^2} \approx \begin{pmatrix} 1 & -2 & 1 \\ -2 & 4 & -2 \\ 1 & -2 & 1 \end{pmatrix} = \begin{pmatrix} 1 \\ -2 \\ 1 \end{pmatrix} \cdot \begin{pmatrix} 1 & -2 & 1 \end{pmatrix},$$

using finite differences in both directions. The final equation of Numerov's method is

$$\frac{1}{h^2} \begin{pmatrix} 1 & 4 & 1 \\ 4 & -20 & 4 \\ 1 & 4 & 1 \end{pmatrix} = \frac{1}{2} \begin{pmatrix} 0 & f_{i+1,j} & 0 \\ f_{i,j-1} & 8f_{i,j} & f_{i,j+1} \\ 0 & f_{i-1,j} & 0 \end{pmatrix} \tag{17}$$

As in the one-dimensional case this approximation leads to an accuracy of $\mathcal{O}(h^4)$. Every mixed derivative in two dimensions can be approximated analogously to the fourth derivative shown above. The resulting stencil can be calculated easily. Given is the stencil $a \in \mathbb{R}^{n\times 1}$for the derivative in the x-direction and the stencil $b \in \mathbb{R}^{1\times m}$ for the y-direction. The mixed derivative is then approximated by $a \cdot b \in \mathbb{R}^{n\times m}$. The accuracy of the mixed approximation is limited by the lower accuracy of their individual one-dimensional ones, given in table 1. Prior to deriving the novel approach to the 2D-Numerov method the form of the matrix has to be clarified. The $N \times M$ grid is represented by a vector. Entry $\psi_{i,j}$ is stored on position $i \cdot N + j$. With this technique two-dimensional wavefunctions can be calculated via the same eigenvalue approach as in the one-dimensional case. The matrices $\mathbb{A}$ and $\mathbb{B}$ in this case are block matrices, consisting of blocks of the size $M \times M$. This single blocks are only filled close to to the diagonal as well as only blocks near the diagonal are filled. Thus the resulting $\mathbb{A}$ matrix is sparsely filled.

Starting with equation (16) a 2D-Numerov method with a certain accuracy can be created. This is shown exemplarily deriving an approach with an accuracy of $\mathcal{O}(h^6)$. Higher accuracy can be

View Article Online
DOI: 10.1039/C6CP06698D

achieved analogously. Choosing $n = 3$ in equation (16) leads to the truncated series expression

$$2f_{i,j}\psi_{i,j} = \frac{\psi_{i+1,j+1} + \psi_{i+1,j-1} + \psi_{i-1,j+1} + \psi_{i-1,j-1} - 4\psi_{i,j}}{h^2} - \frac{4h^2}{4!}\left(\frac{\partial^4\psi}{\partial x^4} + 6\frac{\partial^4\psi}{\partial x^2\partial y^2} + \frac{\partial^4\psi}{\partial y^4}\right) - \frac{4h^4}{6!}\left(\frac{\partial^6\psi}{\partial x^6} + 15\frac{\partial^6\psi}{\partial x^4\partial y^2} + 15\frac{\partial^6\psi}{\partial x^2\partial y^4} + \frac{\partial^6\psi}{\partial y^6}\right) + \mathcal{O}(h^6).$$

In the next step all derivates on the right side are approximated using the respective finite difference expressions. The approximations have to be choosen in a way that the whole equation has the accuracy $\mathcal{O}(h^6)$. The fourth derivatives need the accuracy $\mathcal{O}(h^4)$ and the sixth derivatives require $\mathcal{O}(h^2)$. By the multiplication with h^2 and h^4 respectively the desired accuracy is obtained. After summation of all finite difference contributions the associated 2d-stencil is obtained

$$\begin{pmatrix} 0 & 0 & 0 & 0 & 0 & 0 & 0 \\ 0 & 0 & 0 & 0 & 0 & 0 & 0 \\ 0 & 0 & 0 & 0 & 0 & 0 & 0 \\ 0 & 0 & 0 & f_{i,j} & 0 & 0 & 0 \\ 0 & 0 & 0 & 0 & 0 & 0 & 0 \\ 0 & 0 & 0 & 0 & 0 & 0 & 0 \\ 0 & 0 & 0 & 0 & 0 & 0 & 0 \end{pmatrix} = \frac{1}{2h^2}\begin{pmatrix} 0 & 0 & 0 & 0.0222 & 0 & 0 & 0 \\ 0 & -0.0069 & 0.0278 & -0.3417 & 0.0278 & -0.0069 & 0 \\ 0 & 0.0278 & -0.1111 & 3.1667 & -0.1111 & 0.0278 & 0 \\ 0.0222 & -0.3417 & 3.1667 & -11.1389 & 3.1667 & -0.3417 & 0.0222 \\ 0 & 0.0278 & -0.1111 & 3.1667 & -0.1111 & 0.0278 & 0 \\ 0 & -0.0069 & 0.0278 & -0.3417 & 0.0278 & -0.0069 & 0 \\ 0 & 0 & 0 & 0.0222 & 0 & 0 & 0 \end{pmatrix}. \tag{18}$$

In this case the biggest stencils that appear are the approximations of the fourth and sixth derivatives and regard seven gridpoints. Other stencils approximating the mixed derivatives use only three or five gridpoints.

Also other stencils can be used to approximate the derivations as long as they lead to the desired or a higher accuracy. The accuracy of the whole method is always limited by the term with the largest error. In this case the 7-point stencil of the fourth and sixth derivatives would limit the accuracy to $\mathcal{O}(h^6)$ even if the mixed derivatives were approximated with higher accuracy. Increasingly accurate approaches can be derived analogously thus resulting in larger stencils. As one can easily see, equation (18) leads to the identity matrix on the left side, while the $\mathbb{A}$-matrix is a sparse filled,

View Article Online
DOI: 10.1039/C6CP06698D

derivative	order	−5	−4	−3	−2	−1	0	1	2	3	4	5
2	2	0	0	0	0	1	−2	1	0	0	0	0
2	4	0	0	0	$-\frac{1}{12}$	$\frac{4}{3}$	$-\frac{5}{2}$	$\frac{4}{3}$	$-\frac{1}{12}$	0	0	0
2	6	0	0	$\frac{1}{90}$	$-\frac{3}{20}$	$\frac{3}{2}$	$-\frac{49}{18}$	$\frac{3}{2}$	$-\frac{3}{20}$	$\frac{1}{90}$	0	0
2	8	0	$-\frac{1}{560}$	$\frac{8}{315}$	$-\frac{1}{5}$	$\frac{8}{5}$	$-\frac{205}{72}$	$\frac{8}{5}$	$-\frac{1}{5}$	$\frac{8}{315}$	$-\frac{1}{560}$	0
2	10	$\frac{1}{3150}$	$-\frac{5}{1008}$	$\frac{5}{126}$	$-\frac{5}{21}$	$\frac{5}{3}$	$-\frac{5296}{1800}$	$\frac{5}{3}$	$-\frac{5}{21}$	$\frac{5}{126}$	$-\frac{5}{1008}$	$\frac{1}{3150}$
4	2	0	0	0	1	−4	6	−4	1	0	0	0
4	4	0	0	$-\frac{1}{6}$	2	$-\frac{13}{2}$	$\frac{28}{3}$	$-\frac{13}{2}$	2	$-\frac{1}{6}$	0	0
4	6	0	$\frac{7}{240}$	$-\frac{2}{5}$	$\frac{169}{60}$	$-\frac{122}{15}$	$\frac{91}{8}$	$-\frac{122}{15}$	$\frac{169}{60}$	$-\frac{2}{5}$	$\frac{7}{240}$	0
4	8	$-\frac{41}{7560}$	$\frac{1261}{15120}$	$-\frac{541}{840}$	$\frac{4369}{1260}$	$-\frac{1669}{180}$	$\frac{1529}{120}$	$-\frac{1669}{180}$	$\frac{4369}{1260}$	$-\frac{541}{840}$	$\frac{1261}{15120}$	$-\frac{41}{7560}$
6	2	0	0	1	−6	15	−20	15	−6	1	0	0
6	4	0	$-\frac{1}{4}$	3	−13	29	$-\frac{75}{2}$	29	−13	3	$-\frac{1}{4}$	0
6	6	$\frac{13}{240}$	$-\frac{19}{24}$	$\frac{87}{16}$	$-\frac{39}{2}$	$\frac{323}{8}$	$-\frac{1023}{20}$	$\frac{323}{8}$	$-\frac{39}{2}$	$\frac{87}{16}$	$-\frac{19}{24}$	$\frac{13}{240}$
8	2	0	1	−8	28	−56	70	−56	28	−8	1	0
8	4	$-\frac{1}{3}$	$\frac{13}{3}$	−23	68	−126	154	−126	68	−23	$\frac{13}{3}$	$-\frac{1}{3}$
10	2	1	−10	45	−120	210	−252	210	−120	45	−10	1

Table 1: The finite difference coefficients for several derivatives and several orders. The approximation of the nth derivative has to be divised by the respective h^n term.

symmetric, block matrix. The single blocks are then filled like the matrix in the one-dimensional case with $\mathbb{V}$ again being a diagonal matrix. Diagonalisation of the resulting $\mathbb{H}$ matrix yields the eigenvalues E and the associated two-dimensional wavefunctions.

The derivation of the threedimensional case is analogous to the twodimensional case and shown in the supplementary material.

2.2 Sparsity analysis

The improved Numerov method presented in section 2.1 leads to a sparse matrix $\mathbb{A}$. In this section the sparsity of the resulting matrices in one, two and three dimensions is adressed. The calculations are done for the stencils derived in section 2.1, where a 7-point stencil was used. In all dimensions also an upper estimation is given for a general s-point stencil.

View Article Online
DOI: 10.1039/C6CP06698D

Given is a $N \times M \times L$ grid, where in the one-dimensional case only N is considered as well as $N \times M$ in the two-dimensional case. In one dimension the number of non-zero entries n_{nz} is given by

$$n_{nz} = 7N - 12. \tag{19}$$

Using a stencil regarding s-points yields a number of non-zero entries of

$$n_{nz}(s) = sN - \frac{s^2 - 1}{4}. \tag{20}$$

The sparsity of matrix $\mathbb{A}$ regarding different numbers of gridpoints is presented in table 2. While the size of the matrix problem scales with N^2, the number of non zero entries is proportional to N.

In the two-dimensional case more gridpoints have to be regarded in order to achieve the same

N	N^2	n_{nz}	percentage n_{nz}
10	100	58	58.00000
50	2500	338	13.52000
100	10000	688	6.88000
500	250000	3488	1.39520
1000	1000000	6988	0.69880
5000	25000000	34988	0.13995
10000	100000000	69988	0.06999

Table 2: Percentage of non-zero entries n_{nz} in one dimension with various gridpoints N.

accuracy. So the two-dimensional matrices with the same size as the one-dimensional ones have more non-zero entries. The number of non-zero entries of a resulting two-dimensional matrix using a 7-point stencil is

$$n_{nz} = 29NM - 36N - 36M + 36. \tag{21}$$

For a stencil regarding s-points the number of non-zero entries is given by

$$n_{nz}(s) = NM\left(s^2 - 5s + 8\right) - N\left(\frac{s^3 - 6s^2 + 15s - 10}{4}\right) - M\left(\frac{s^3 - 2s^2 + 7s - 6}{8}\right) + \frac{s^4 - 4s^3 + 2s^2 - 3}{32}. \tag{22}$$

View Article Online
DOI: 10.1039/C6CP06698D

In table 3 the percentage of non-zero entries of different sized grids is illustrated. The resulting

N	M	$(NM)^2$	n_{nz}	percentage n_{nz}
10	10	10000	2216	22.16000
25	25	390625	16361	4.18842
50	50	6250000	68936	1.10298
100	100	100000000	282836	0.28284
250	250	3906250000	1794536	0.04594
500	500	62500000000	7214036	0.01154
1000	1000	1000000000000	28928036	0.00289

Table 3: Percentage of non-zero entries n_{nz} in two dimensions with various gridpoints.

matrix in the three-dimensional case has even more non-zero entries than the matrices in the one- or two-dimensional case. This is not surprising due to the higher amount of neighboured gridpoints in three dimensions. The total number of non-zero entries in the three-dimensional case, considering a 7-point stencil, is given by

$$n_{nz} = 67NML - 60(NM + ML + NL) + 36(N + M + L). \tag{23}$$

As the exact estimation of non-zero entries in a matrix using a s-point stencil gets more complicated with increasing dimensions no closed formula for the three-dimensional case was derived, but it can be estimated upwards by

$$n_{nz}(s) \leq \left(N + 2 \sum_{i=1}^{(s-1)/2} (N - i) \right) \cdot \left(M + 2 \sum_{i=1}^{(s-1)/2} (M - i) \right) \cdot \left(L + 2 \sum_{i=1}^{(s-1)/2} (L - i) \right). \tag{24}$$

This estimation is based on the assumption, that the whole $s \times s \times s$ stencil is filled with non-zero entries which is, however, not always the case. The percentage of non-zero entries in the resulting matrices in the three-dimensional case is shown in table 4. It can be seen that the percentage of non-zero entries is decreasing rapidly in all three dimensions. With the same matrix size, the percentage of filled entries is the lowest in the one-dimensional case due to the fewer gridpoints that have to be regarded. The percentage of non-zero entries in tables 2, 3 and 4 give an idea of the reduced memory requirement of a sparse over a dense formulation. Due to this lowered memory

View Article Online
DOI: 10.1039/C6CP06698D

N	M	L	$(NML)^2$	n_{nz}	percentage n_{nz}
10	10	10	1000000	50080	5.00800
25	25	25	244140625	937075	0.38383
50	50	50	15625000000	7930400	0.05075
75	75	75	177978515625	27261225	0.01532
100	100	100	1000000000000	65210800	0.00652
200	200	200	64000000000000	528821600	0.00083
300	300	300	729000000000000	1792832400	0.00025
400	400	400	4096000000000000	4259243200	0.00010
500	500	500	15625000000000000	8330054000	0.00005

Table 4: Percentage of non-zero entries n_{nz} in three dimensions with various gridpoints.

demand it is possible to work with substantially enlarged grids on a standard desktop PC. With 32 GB of memory otherwise the calculations would be limited to gridsizes of 63000, 251×251 or $40 \times 40 \times 40$ points. The estimation above regards only the needed memory to safe one dense matrix with ≈ 63000 entries. Moreover the standard Numerov method requires at least a second matrix which has to be saved, inverted and multiplied with matrix $\mathbb{A}$. Finally, use of sparsity also greatly reduces the memory requirement of routines to find eigenvalues and the respective eigenvectors.

2.3 Computational Methods - Algorithms to solve the matrix eigenvalue problem

Matrix eigenvalue problems such as ones occurring in this work can be solved using basic algebraic methods. A number of frameworks including suitable algorithms are available, e.g. the Gnu Scientific Library (GSL) [19], ARPACK [20], Armadillo [21], MKL [22] libraries. The algorithms for dense matrices to solve the matrix eigenvalue problem in the standard Numerov method have the disadvantage that the compuational demand grows exponentially with increasing matrix size, inter alia because all eigenstates are computed. This leads to significantly higher computational amount for bigger grids, especially in higher dimensions. Combined with the high memory demand this represents the disadvantages of the standard Numerov method as outlined earlier.

As the improved Numerov method uses sparse matrices, suitable algorithms have to be used to

View Article Online
DOI: 10.1039/C6CP06698D

take advantage of the sparse character leading to a manageable computational demand. Since the gridsize in the one-dimensional case is generally low, the use of sparse algorithms showed to be not favorable for matrices up to 2000 gridpoints. The respective results proofed to be more accurate using dense algorithms. For this purpose the Gnu Scientific Library (GSL) [19] was used. Sparse algorithms were found to lead to slightly worse results. This can be due to the iterative character of the methods or due to the shape of the matrix where only the elements near the diagonal are non-zero values.

In two and three dimensions also few gridpoints per dimension lead to big matrices. Grids with 150×150 points need hours to calculate all eigenvalues using the GSL-routines. In this cases the sparse algorithm of the ARPACK Armadillo library was used, restricting the eigenvalue search to the lowest states only. So the same calculations take only a few minutes requiring far less memory than in the dense case.

2.4 Test-Systems

In this section the investigated quantum systems are presented. The results of the respective calculations are discussed in section 3. If not explicitely mentioned the reduced mass was assumed to be 1.0 u. All quantum mechanical calculations were performed using Gaussian09 D.01 [23].

In the one-dimensional case three different systems were investigated. Two systems to show the accuracy of the method and one system to show an example for its application. The first example is a harmonic oscillator with a force constant of $k = 1098.018 \frac{kcal}{mol\mathring{A}^2}$ in the interval $[-2.5\mathring{A}, 2.5\mathring{A}]$. In order to investigate the accuracy of the method different gridsizes from 51 to 1001 points were employed. The odd number of gridpoints was chosen to include a gridpoint at the minimum of the potential. Furthermore, the constant k was derived from the mean value of the asymmetric and symmetric vibrational frequency of the H_2O molecule, given in [24]

As a second example a Morse potential

$$V(x) = A\Big(1 - exp(-\alpha x)\Big)^2$$

View Article Online
DOI: 10.1039/C6CP06698D

was investigated, with $A = 174.147\frac{kcal}{mol}$ and $\alpha = 1.776\frac{1}{\mathring{A}}$. The Morse potential was fitted so that its curvature and that of the harmonic oscillator are equal at the equilibrium position. An interval of $[-1.5\mathring{A}, 2.5\mathring{A}]$ was considered. Also in this case different gridsizes between 51 and 1001 points were calculated.

In addition to the two examples for whom analytical solutions exist a third example was considered to demonstrate an application of the method. For this purpose the potential of molecular hydrogen H_2 was calculated. The distance between the two atoms was varied equidistantly with $h = 0.025\mathring{A}$. Since H_2 posses only two electrones, configuration interaction (CI) using single and double excitations (CISD) already corresponds to Full-CI. Three different Dunning-type basis sets (cc-pVDZ, cc-pVTZ and cc-pVQZ) have been employed [26].

In the two-dimensional case two different systems were investigated. The first example was a two-dimensional harmonic oscillator with $k_x = 1000\frac{kcal}{mol\mathring{A}^2}$ and $k_y = 750\frac{kcal}{mol\mathring{A}^2}$ in the area $[2.0\mathring{A}, 2.0\mathring{A}] \times [2.0\mathring{A}, 2.0\mathring{A}]$. The spring constant was chosen in order to approximate an O-H binding in the x-direction. The constant in the y-direction was lowered to split up the energy levels in the different dimensions. Various gridsizes between 21×21 and 601×601 points were calculated. Thus the biggest grid contains 361201 single gridpoints. In this case the standard Numerov method using dense matrix algorithms would lead to a matrix with more than 130 billion entries and therefore to a high computational demand as well as huge memory demand, of approximately one terabyte.

In the second example the tunneling splitting of the proton transfer reaction in malonaldehyde was investigated. It is an example of multidimensional tunneling and a well studied system. For this purpose the position of the hydrogen atom was varied in the area highlighted in figure 5a calculating a 36×45 grid via DFT using the B3LYP functional [27] with the 6-311g(d,p) basis set [28]. In this test case the remaining part of the molecule was considered rigid. Intuitively, one would consider the configuration of the transition state as a representative configuration. However, according to the respective 2d-potential energy scan (cf. figure S1) the double-well character is almost non-existent. The respective energy barrier was found to be only about approx. 0.3 kcal/mol being even lower than k_BT at room temperature. For this reason the minimum configuration was chosen. This can be justified by considering the tunnelling process of the light proton as a fast event compared to

View Article Online
DOI: 10.1039/C6CP06698D

the rearrangement of the back-bone of malonaldehyde, which due to the presence of five heavy atoms (*i.e.* carbon and oxygen) can be expected to occur on a much longer time scale. This point of view assumes that the symmetric configuration of the molecule is only obtained as a transition configuration during the relaxation of the molecue but not in the moment of the tunneling. Thus, the relaxation occurs after the tunneling event which then leads to a minimum configuration similar to the starting configuration.

Using the respective potential obtained from a 2d-scan in the molecular plane the nuclear wavefunctions of the proton was calculated. The gridsize was chosen as 0.05 Å and the mass of the hydrogen atom was set to 1.007825032 u.

Because the potential surface resulting from the asymmetric configuration leads to a distortion of the wavefunction towards the more stable minimum, an additional system resembling a text book example has been investigated as well. Here, a double-well potential was combined with an harmonic oscillator in the other dimension in order to show an example for tunneling splitting of a symmetrized potential in the absence of mode coupling. The data of this potential is not given because it was only considered to demonstrate the shape of the wavefunctions if the motion in the different dimensions is uncoupled.

For the three-dimensional case only one example was considered, namely the 3d-coupled normal mode vibrations of a water molecule considering two different isotopologues (H_2O, D_2O and T_2O). Starting with a CCSD(T)/aug-cc-pVQZ harmonic frequency evaluation of the water molecule in its minimum geometry [26,29], the three normal modes and the respective reduced masses are obtained. Next, the three-dimensional potential along the three normal modes can be investigated simultaneously using mass weighted coordinates. This is necessary to achieve an equispaced grid because the reduced mass is slightly different for each degree of freedom. For H_2O and D_2O a $66 \times 97 \times 53$ grid was considered, with 66 points for the symmetric stretch mode, 97 points for the bending mode and 53 points for the asymmetric stretch mode. The respective intervals are $[-0.4\mathring{A}, 0.9\mathring{A}]$, $[-0.943\mathring{A}, 0.943\mathring{A}]$ and $[-0.511\mathring{A}, 0.511\mathring{A}]$. All computations have been executed without application of the frozen core approximation.

The separate investigation of the heavy isotopologues D_2O and T_2O enables the analysis of the

View Article Online
DOI: 10.1039/C6CP06698D

vibrational frequency under consideration of anharmonicity and mode-mode coupling, while at the same time the influence of nuclear quantum effects is eliminated to a large extend, whereas in the case of H_2O all three contributions influence the final wavenumbers. Since the energy levels of T_2O can be expected to be approximately a factor 3 smaller than in the H_2O case, the size of the grid could be reduced to $51 \times 75 \times 41$. The respective intervals are $[-0.3\mathring{A}, 0.7\mathring{A}]$ for the symmetric stretch mode, $[-0.723\mathring{A}, 0.723\mathring{A}]$ for the bending mode and $[-0.386\mathring{A}, 0.386\mathring{A}]$ for the asymmetric stretch mode. In both cases the symmetric stretch mode corresponds to the lightest mass. For this mode a grid spacing of 0.02Å was considered. A smaller spacing was applied to the bending and the asymmetric stretch mode to guarantee an equispaced grid regarding mass-weighting.
Application of the 3D-Numerov approach then yields the fundamental vibrational frequencies under consideration of anharmonicity, quantum tunnelling as well as mode-mode coupling.

3 Results

In this section results of the test-systems presented in section 2.4 are discussed, demonstrating the performance of the modified Numerov method in one, two and three dimensions. In one dimension the modified method also was compared to an implementation of the standard Numerov technique of different accuracy. In this case for all calculations the dense algorithms of the GSL library [19] were used. The reformulation without $\mathbb{B}$ matrix is not particularly relevant due to the low runtime of the standard Numerov in one dimension. The concept can be extended to higher dimensions, however, with big advantage of the inherent sparse character of the modified approach. In two and three dimensions the sparse algorithms of the ARPACK Armadillo library [21] were used. In higher dimensions only the performance of the improved Numerov method was tested.

3.1 One dimension

In one dimension three different systems were investigated as outlined in section 2.4. The results of the deviation of the predicted energy levels from the analytical solution for harmonic and Morse

View Article Online
DOI: 10.1039/C6CP06698D

oscillators are presented in figures 1 and 2, comparing the improved Numerov method of different accuracy with the respective standard Numerov implementation. The approach with higher accuracy was constructed following [14]. It can be seen that the lowest error is achieved for the lowest eigenvalue and increases with higher eigenvalues. Both approaches using the same stencil size lead to very similar deviations from the analytical eigenvalue. However, the computational effort for the standard Numerov methods is higher due to the computation of $\mathbb{B}^{-1}$ and $\mathbb{B}^{-1}\mathbb{A}$ as discussed earlier. Plotting the logarithm of the gridsize h versus the logarithm of the deviation from the exact result leads to a line with the gradient equal to the order of the used stencil. The corresponding plots are given in the supplementary material (cf. figure S2, S3). In this section only the resulting gradients of all calculated cases are given in table 5. It is shown that in both examples all stencils perform well. The higher stencils do not reach the theoretical order completely. This can be due to round off errors during the computational process, regarding the higher amount of non-zero entries when using higher stencils.

Theoretical order ($\mathcal{O}(h^n)$)	2	4	6	8	10	12
harmonic potential	2.0	4.0	5.9	7.9	9.8	11.7
Morse potential	2.0	4.0	5.9	7.9	9.7	11.4

Table 5: The resulting order of the different stencil sizes of the adapted Numerov method for both onedimensional analytical examples. The values were computed via regression of the linear part of the double-logarithmic plot (fig. S2,S3.

The third example considered in this paper is the hydrogen molecule and its isotopologues HD and D_2. The resulting frequencies are summarised in table 6 which improve significantly with increasing basis. The best data obtained at the aug-cc-pVQZ level is in excellent agreement with experimental results, the highest error was 1.0 cm^{-1} for the fundamental vibration and 2.5 $cm^{-1}$for the first overtone. In figure 3 all bounded states of the H_2 molecule are shown. For all calculations of the molecules the improved Numerov method with a 7-point stencil was used. As it can be seen in 1 and 2 using a higher stencil would not improve the result with the given spacing of 0.025 Å because for this application only an accuracy of $\approx 10^{-4}$ is needed.

The results in the one-dimensional case show that the improved Numerov method performs as well

View Article Online
DOI: 10.1039/C6CP06698D

as the standard Numerov implementation with the advantage that no inverse matrix has to be calculated and computational as well as memory demands are lowered when using sparse matrices and the respective algorithms. This property becomes more advantageous in higher dimensions discussed in the following.

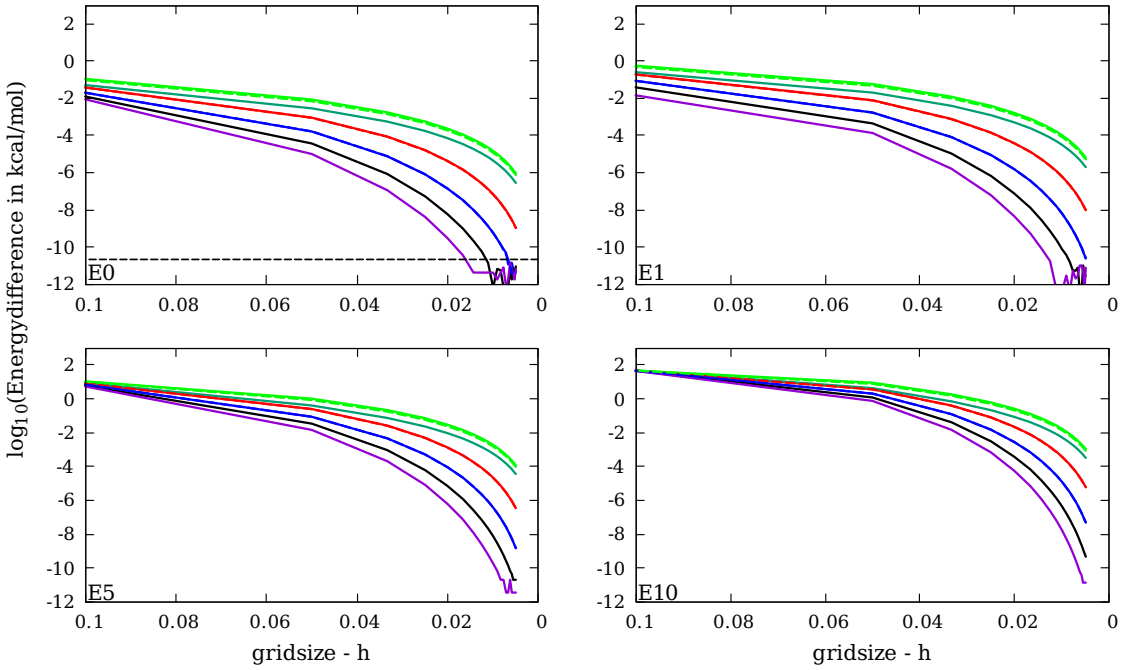

Figure 1: Ground state, first, fifth and tenth exited state of the harmonic oscillator in one dimension. Standard Numerov $\mathcal{O}(h^4)$ - dark green (3-point), $\mathcal{O}(h^4)$ - dashed green (5-point), $\mathcal{O}(h^6)$ - dashed red, $\mathcal{O}(h^8)$ - dashed blue.
Improved Numerov: $\mathcal{O}(h^4)$ - green, $\mathcal{O}(h^6)$ - red, $\mathcal{O}(h^8)$ - blue, $\mathcal{O}(h^{10})$ - black, $\mathcal{O}(h^{12})$ - violet.
The dashed lines are nearly congruent to the continuous lines and therefore barely visible.

3.2 Two dimensions

As a first example a two-dimensional harmonic oscillator was investigated in order to validate the accuracy of the method and the used algorithms in higher dimensions. Looking at the gridsize in figure 4 one can see that the results of the improved Numerov method in two dimensions are comparable to the one-dimensional case. Obviously the same gridsize in two dimensions leads to

View Article Online
DOI: 10.1039/C6CP06698D

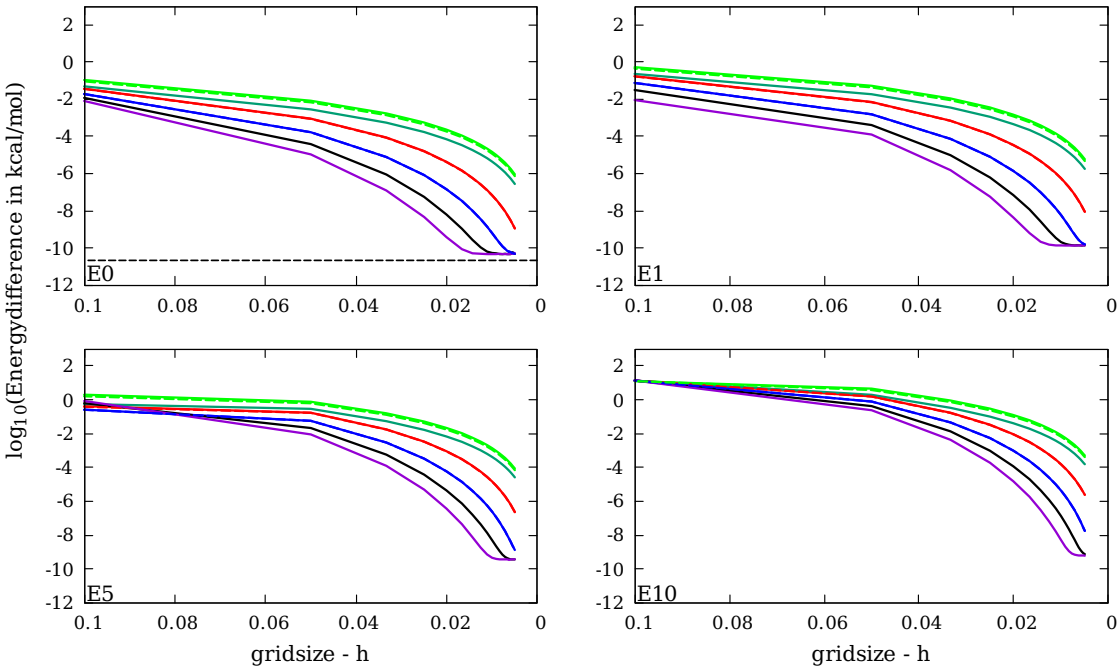

Figure 2: Ground state, first, fifth and tenth exited state of the Morse potential in one dimension.Standard Numerov $\mathcal{O}(h^4)$ - 3-point(dark green), $\mathcal{O}(h^4)$ - 5-point (dashed green), $\mathcal{O}(h^6)$ (dashed red), $\mathcal{O}(h^8)$(dashed blue).
Improved Numerov: $\mathcal{O}(h^4)$ (green), $\mathcal{O}(h^6)$ (red), $\mathcal{O}(h^8)$ (blue), $\mathcal{O}(h^{10})$ (black), $\mathcal{O}(h^{12})$(violet).
The dashed lines are nearly congruent to the continuous lines.

a significant higher number of gridpoints than in the one-dimensional case. Analogously to the one-dimensional case a double-logarithmic plot leads to a line with the gradient equal to the order of the used stencil. The corresponding plot is given in the supplementary material (cf. figure S4) . In this section only the resulting gradients of all calculated cases are given in table 7. It is shown that all stencils perform well. Again higher stencils do not reach the theoretical order completely, which can be explained by round off errors during the computational process, regarding the higher amount of non-zero entries when using higher stencils.

In the second example the tunneling splitting of the hydrogen atom in malonaldehyde was investigated. After creating a 36×45-point grid at B3LYP/6-311g(d,b) level for a representative geometry energies of the single states and the corresponding wavefunctions were calculated using

View Article Online
DOI: 10.1039/C6CP06698D

		fundamental	1^{st} overtone
cc-pVDZ	H_2	4144.5	8052.4
	HD	3617.3	7057.0
	D_2	2981.0	5843.4
cc-pVTZ	H_2	4165.7	8095.7
	HD	3635.9	7094.0
	D_2	2996.6	5873.7
cc-pVQZ	H_2	4162.1	8089.5
	HD	3632.7	7088.3
	D_2	2993.7	5868.6
exp	H_2	4161.1[a]	8087[b]
	HD	3632.2[a]	7087[b]
	D_2	2993.6[a]	5868.5[b]

Table 6: Fundamental and first overtone frequencies for different molecular hydrogen species at Full CI level obtained from a 7-point Numerov analysis of the potential with $h = 0.025$ Å.
[a] Ref. [30]
[b] Ref. [31]

Theoretical order ($\mathcal{O}(h^n)$)	4	6	8	10
harmonic potential	4.0	5.9	7.9	9.8

Table 7: The resulting order of the different stencil sizes of the adapted Numerov method for the two-dimensional harmonic oscillator. The values were computed via regression of the linear part of the double-logarithmic plot (fig. S4.

the improved Numerov method with an 11-point stencil. The energy difference between the two lowest states is 20.04 cm^{-1}, the respective experimental value was reported as 21.6 cm^{-1} [32]. In figure 5a the potential is shown in the exact position of the molecule. In one direction a double-well potential can be seen, but also the low potential which allows the bound hydrogen atom to rotate partially about the respective oxygen atom. In figure 5 also the wavefunctions corresponding to the first two states are shown. Due to the asymmetry in the structure imposed by considering the proton transfer to be faster than the relaxation of the molecular back-bone (see discussion in section 2.4), the two minima of the potential energy surface do not share the same energy and consequently, different peak amplitudes are observed for the two wavefunctions. The deviation to experimental value of 21.6 cm^{-1} can be explained by the use of only one geometry of the molecular structure as well as the known shortcomings of DFT to describe dispersion interactions.

View Article Online
DOI: 10.1039/C6CP06698D

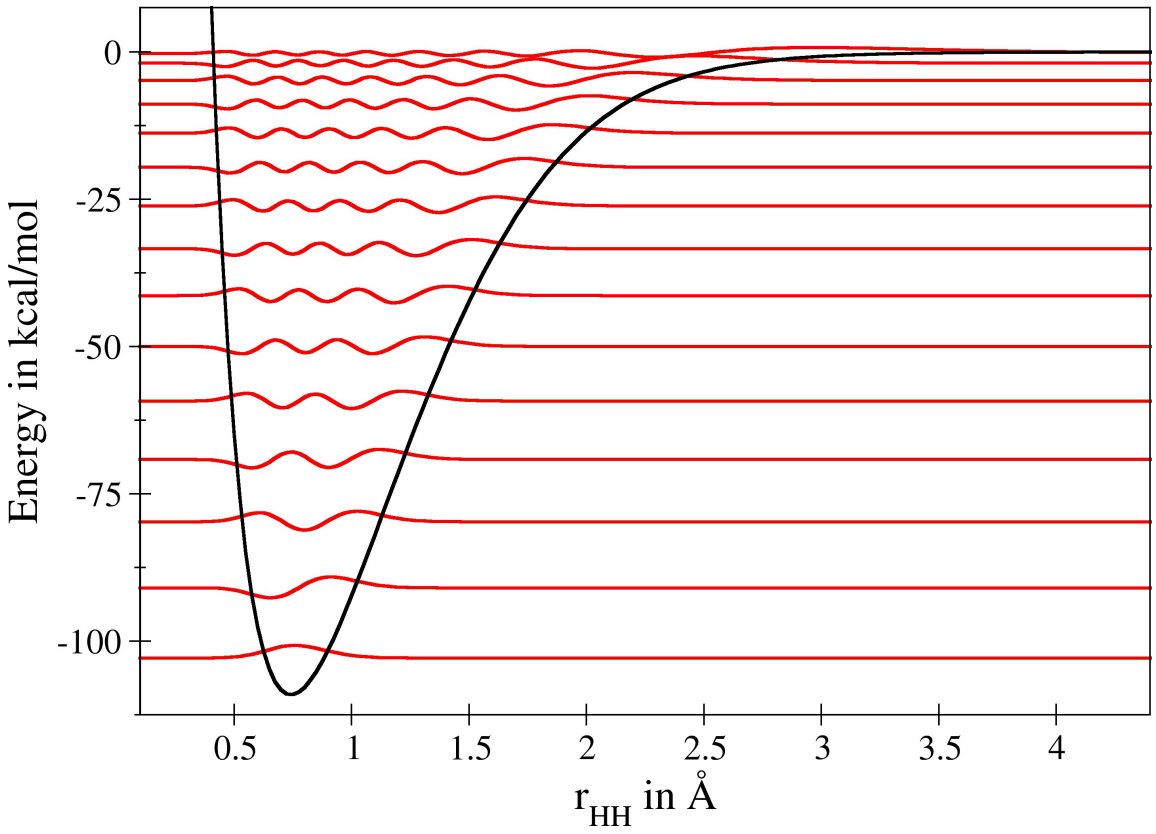

Figure 3: All binding states of the H_2 molecule calculated via FCI/cc-pVQZ

To demonstrate that the Numerov framework predicts wave funtions with equal amplitudes a symmetric, two dimensional double-well potential has been included as an additional example (fig. 5b, 5d and 5f).

3.3 Three dimensions

In the three-dimensional case only one example was considered. The vibrational frequencies of the three normal modes of H_2O and its isotopologues D_2O and T_2O were calculated using a potential created at CCSD(T)/aug-cc-pVQZ level, without application of the frozen core approximation. The results of the calculation are given in table 8. For comparison the results for the harmonic approximation and the 1d-Numerov result is given. In the one-dimensional Numerov calculation each

View Article Online
DOI: 10.1039/C6CP06698D

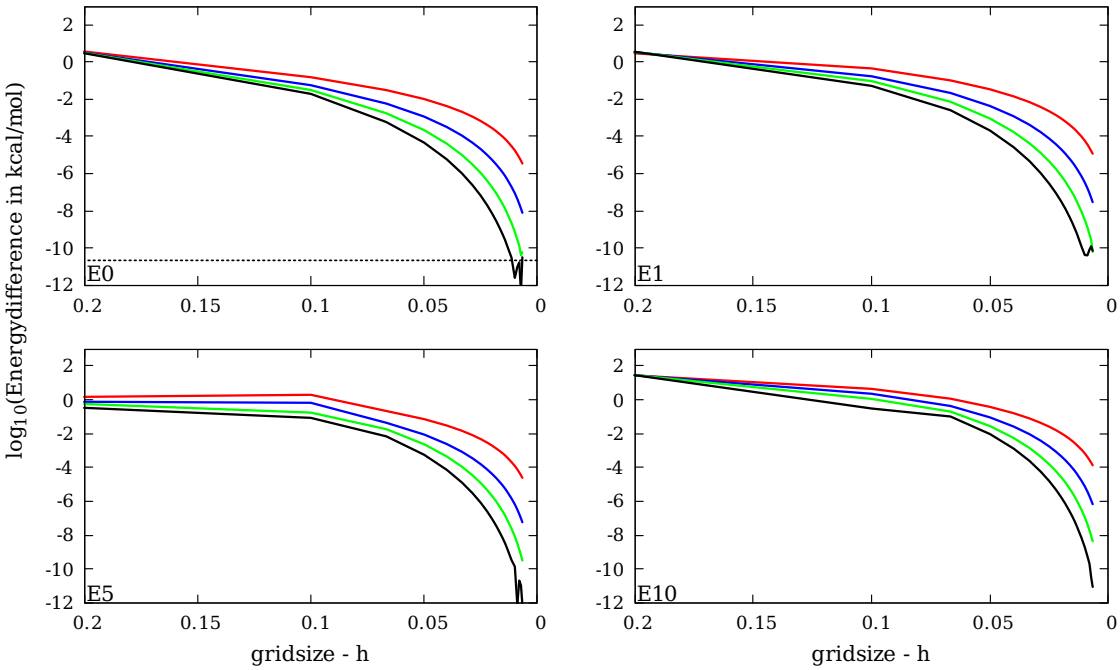

Figure 4: Ground state, first, fifth and tenth exited state of the harmonic oscillator in two dimensions.
Improved Numerov: $\mathcal{O}(h^4)$ - red, $\mathcal{O}(h^6)$ - blue, $\mathcal{O}(h^8)$ - green, $\mathcal{O}(h^{10})$ - black.

normal mode frequency was calculated separately. The large deviation compared to experimental results is due the not considered mode-mode coupling. Using the adapted three-dimensional Numerov method anharmonicity and mode-mode coupling is inherently considered and the respective results are in excellent agreement with the experimental data showing relative deviations of less than 1% in both cases. The deviation of the T_2O frequencies is lower than the one of H_2O and D_2O, which can be explained by the increased influence of nuclear quantum effects in case of the lighter hydrogen isotopes. Further deviation from the experiment results from the neglect of rovibrational coupling, which is typically in the order of a few wavenumbers for small molecules such as water.

View Article Online
DOI: 10.1039/C6CP06698D

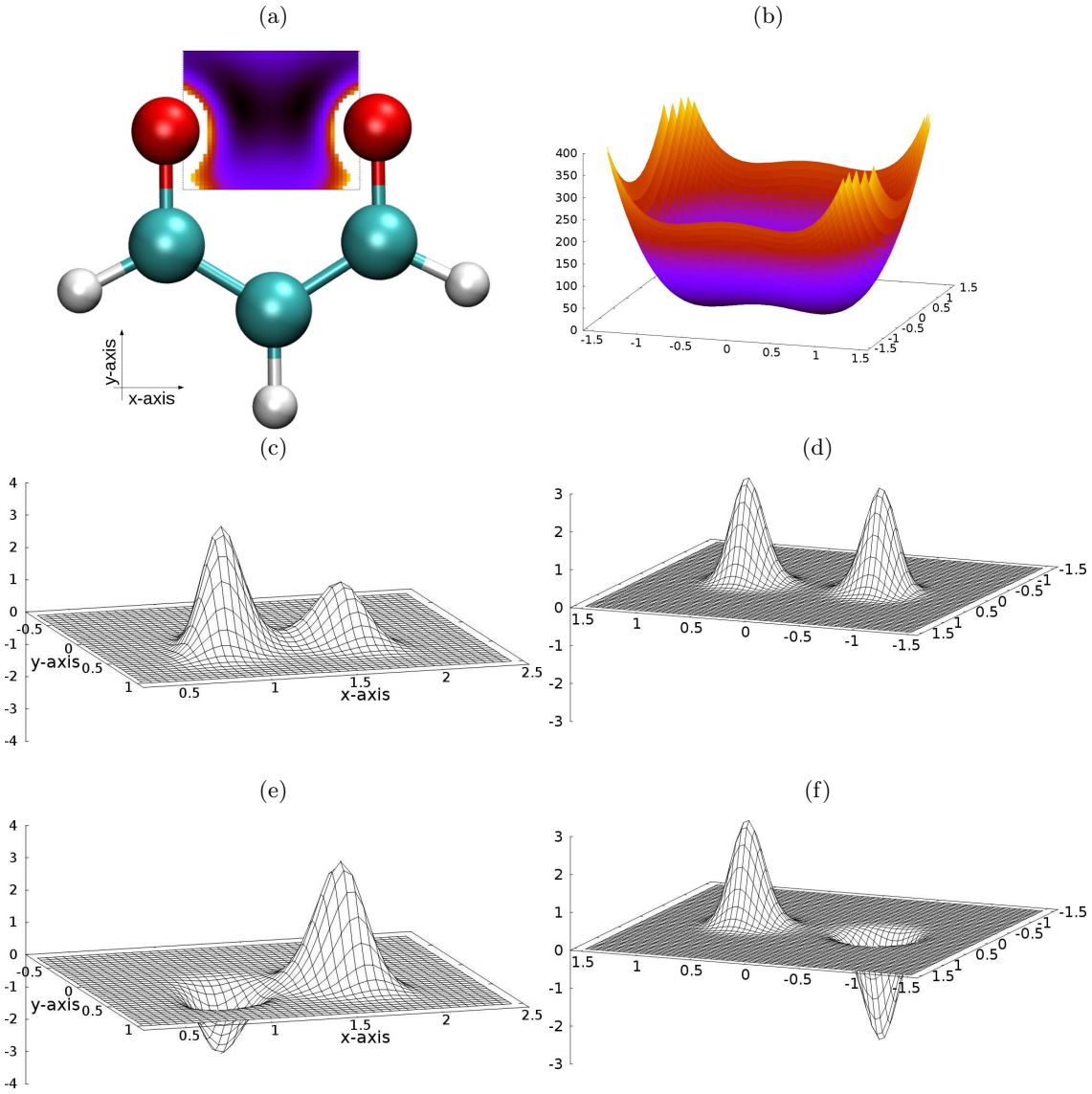

Figure 5: The axis in a) correspond to those in c) and e). The connection line of the O-atoms corresponds to $y = 0$.
a) Malonaldehyde. The scanned area is bounded by the dashed line. The potential is plotted up to 400 kcal/mol. Values above are not plotted.
b) Doublewell potential in x-direction combined with an harmonic oscillator in y direction
c) Wavefunction of the ground state on malonaldehyde
d) Ground state wavefunction of the potential plotted in b)
e) Wavefunction of the first excited state of malonaldehyde
d) First excited state wavefunction of the potential plotted in b)

View Article Online
DOI: 10.1039/C6CP06698D

H_2O						
	δ_b	ν_s	ν_{as}	$\Delta\delta_b$	$\Delta\nu_s$	$\Delta\nu_{as}$
exp[a]	1595	3657	3756			
harmonic	1652	3842	3951	57 (3.5%)	185(5.1%)	195(5.2%)
1d-Numerov	1638	3757	4037	43 (2.7%)	100(2.7%)	281(7.5%)
3d-Numerov	1586	3668	3744	-9 (0.6%)	11(0.3%)	-12(0.3%)
D_2O						
	δ_b	ν_s	ν_{as}	$\Delta\delta_b$	$\Delta\nu_s$	$\Delta\nu_{as}$
exp[b]	1178	2672	2788			
harmonic	1209	2769	2895	31(2.6%)	97(3.6%)	107 (3.8%)
1d-Numerov	1203	2725	2943	25(2.1%)	53 (2.0%)	155(5.6%)
3d-Numerov	1175	2679	2784	-3(-0.3%)	7(0.3%)	-4(-0.1%)
T_2O						
	δ_b	ν_s	ν_{as}	$\Delta\delta_b$	$\Delta\nu_s$	$\Delta\nu_{as}$
exp[c]	995	2237	2367			
harmonic	1017	2306	2444	22(2.2%)	69(3.0%)	77(3.3%)
1d-Numerov	1014	2275	2478	19(1.8%)	38(1.7%)	111(4.7%)
3d-Numerov	994	2243	2365	-1 (-0.2%)	6 (0.25%)	-2 (-0.08%)

Table 8: Vibrational mode frequencies for H_2O, D_2O and T_2O at CCSD(T)/aug-cc-pVQZ level without frozen core approximation obtained from a 9-point Numerov analysis of the potential with $h = 0.02\mathring{A}$. All frequencies are given in 1/cm.
[a] Ref. [24]
[b] Ref. [25]
[c] Ref. [33–35]

View Article Online
DOI: 10.1039/C6CP06698D

4 Conclusions

In this paper an adapted Numerov method with arbitrary accuracy was presented. A detailed analysis of the respective Taylor-series enabled the formulation of an adapted approach in which the calculation of $\mathbb{B}^{-1}\mathbb{A}$ is no longer neccesary. In addition, the resulting $\mathbb{A}$ matrix is symmetric and sparse filled. Utilising the sparse character of the matrix the memory requirements can be significantly lowered while the use of sparse type algorithms reduces the computational demand. Finally, the use of symmetric matrices has a further important advantage: its eigenvalues are guaranteed to be real and the respective eigenfunctions are orthogonal to each other, crucial properties for energy levels and the corresponding wavefunctions.

Overall it was demonstrated, that the resulting accuracy depends mainly on the gridspacing and not on the dimension of the problem. In tables 5 and 7 it was shown that the improved Numerov method nearly reaches the theoretical order in analytical examples. Figures 1, 2 and 4 highlight the required gridspacing to achieve a particular accuracy. For instance in case of the two-dimensional harmonic oscillator the size of the grid can be enlarged from approx. 0.02 to 0.05 Å when moving from a five-point to an eleven-point stencil to achieve an accuracy of at least 10^{-4}, thus reducing the number of grid points by more than a factor of two per dimension.

The key advantage of the newly derived modification of the Numerov approach results from the exploitation of matrix symmetry in conjunction with the performance of sparse algorithms, thus not only greatly reducing memory and CPU requirements but at the same time ensuring the correct properties of the resulting wavefunctions. Since the performance of the improved Numerov method depends solely on the spacing of the grid in conjunction with the size of the chosen stencil, the quality of the potential energy surface is the remaining factor determining the accuracy of results. Exemplary applications of quantum systems in one, two and three dimensions have been presented. In addition to providing a good estimation of the tunnelling splitting of the H-transfer in malonaldehyde, the adapted Numerov method was shown to consider anharmonicity, mode-mode coupling and nuclear quantum effects with high accuracy. In case highly accurate quantum chemical methods

View Article Online
DOI: 10.1039/C6CP06698D

can be applied as has been done in this work for molecular hydrogen as well as the water molecules, agreement with experimental data within 1% can be achieved for all isotopologues investigated.

In typical applications two possibile scenarios to create the required potential data have to be considered: The grid can be either generated evaluating an analytical potential-function (e.g. a double-well potential) or by a QM- or MM-based energy calculation for every single configuration. In the second case the calculation of the grid can be expected much more time consuming than the calculation of the eigenstates. For instance, assuming the computation time for one data point as 1 minute the construction of a 30×30 grid needs 15 hours. Afterwards the improved Numerov method computes the eigenvalues and eigenvectors in less than a minute. In this case the use of a large stencil is of advantage to dramatically reduce the required grid-size. This is of particular benefit in two- and three-dimensional applications. The run-time of the improved Numerov method does not change much using a higher stencil, since it scales more dominantly with the number of datapoints. If on the other hand the grid is created evaluating a known potential-function the main part of the computation rests with the determination of the eigenvectors and eigenvalues. In this case larger grid-sizes can be easily constructed and the sparse properties of the modified Numerov framework are of particular advantage. In both cases the number of gridpoints is the limiting factor but in a different way.

This problem strikes mainly problems in higher dimensions. Therefore, using a larger stencil to reach the same accuracy with less gridpoints is particular advantage. To keep the sparse character of a matrix it is recommended to work with at least twice as much gridpoints as the used stencil length.

The number of gridpoints and the chosen gridsize h depend on the aim of the computation (accurate energy levels vs. tightly-spaced wavefunctions), whereby more gridpoints don't necessarily lead to a smaller gridsize: special care has to be taken in investigating eigenstates near the lower energy limit on the boundary of the grid. In case a state is close to the boundary poor results might be obtained, thus requiring an extension of the grid. Although the error of the eigenvalues may not be very significant, the resulting eigenfunctions may be strongly infuenced, since they do not sufficiently approach zero at the boundary.

View Article Online
DOI: 10.1039/C6CP06698D

5 Acknowledgement

The research was financially supported by *Verein zur Förderung der wissenschaftlichen Ausbildung und Tätigkeit von Südtirolern an der Landesuniversität Innsbruck*. This work was supported by the Austrian Ministry of Science BMWFW as part of the Konjunkturpaket II of the Focal Point Scientific Computing at the University of Innsbruck.

References

[1] E. Schrödinger. Quantisierung als Eigenwertproblem. *Annalen der Physik*, 79:361, 489, 734, 1926.

[2] C. E. Dykstra and D. J. Malik. Derivative numerov–cooley theory. a method for finding vibrational state properties of diatomic molecules. *Journal of Chemical Physics*, 87:2807, 1987.

[3] Y. Futami, Y. Ozaki, and Y.Ozaki. Absorption intensity changes and frequency shifts of fundamental and first overtone bands for oh stretching vibration of methanol upon methanol-pyridine complex formation in ccl4: analysis by nir/ir spectroscopy and dft calculations. *Physical Chemistry Chemical Physics*, 18:5580, 2016.

[4] S.K. Gregurick, G.M. Chaban, and R.B. Gerber. Ab initio and improved empirical potentials for the calculation of the anharmonic vibrational states and intramolecular mode coupling of n-methylacetamide. *The Journal of Physical Chemistry A*, 106(37):8696–8707, 2002.

[5] M. Bounouar and Ch. Scheurer. Reducing the vibrational coupling network in n-methylacetamide as a model for ab initio infrared spectra computations of peptides. *Chemical Physics*, 323(1):87 – 101, 2006.

View Article Online
DOI: 10.1039/C6CP06698D

[6] W.H. Press, S. Teukolsky, W.T. Vetterling, and B. P. Flannery. *Numerical Recipes. The Art of Scientific Computing*. Cambridge University Press, 2007.

[7] Matrix numerov method for solving schrödinger's equation. *American Journal of Physics*, 80:1017, 2012.

[8] B.V. Numerov. Méthode nouvelle de la détermination des orbites et le calcul des éphémé rides en tenant compte des perturbations. *Publications de l'Observatoire Astrophysique Central de Russie*, 2:188–288, 1923.

[9] B.V. Numerov. A method of extrapolation of perturbations. *Monthly Notices Royal Atronomical Society*, 84:592–601, 1924.

[10] B. Fornberg. Generation of finite difference formulas on arbitrarily spaced grids. *Mathematics of Computation*, 51(184):699–706, 1988.

[11] H. Grubmüller T. Graen. Nusol — numerical solver for the 3d stationary nuclear schrödinger equation. *Computer Physics Communications*, 198:169 – 178, 2016.

[12] M. Eckert. Solving the 1-, 2- and 3-dimensional schrödinger equation for multiminima potentials using the numerov-cooley method. an extrapolation for energy eigenvalues. *Journal of Computational Physics*, 82:147–160, 1989.

[13] B.R. Johnson. New numerical methods applied to solving the one-dimensional eigenvalue problem. *Journal of Chemical Physics*, 67:4086, 1977.

[14] D. Tang. *Generalized Matrix Numerov Solutions to the Schrödinger Equation*. National University of Singapore, Bachelor thesis, April 2014.

[15] J.C. Mason and D.C. Handscomb. *Chebyshev Polynomials*. CRC Press, 2010.

[16] B. Fornberg. *A Practical Guide to Pseudospectral Methods*. Cambridge University Press, 1998.

[17] D.T. Colbert and W.H. Miller. A novel discrete variable representation for quantum mechanical reactive scattering via the s-matrix kohn method. *Journal of Chemical Physics*, 96(3):1982–1991, 1992.

View Article Online
DOI: 10.1039/C6CP06698D

[18] A. Bulgac and M. McNeil Forbes. Use of the discrete variable representation basis in nuclear physics. *Physical Review C*, 87, 2013.

[19] Brian Gough. *Gnu Scientific Library Reference Manual - Third Edition*. Network Theory Ltd., 2009.

[20] R. B. Lehoucq, D. C. Sorensen, and C. Yang. *ARPACK Users Guide: Solution of Large-Scale Eigenvalue Problems with Implicitly Restarted Arnoldi Methods*. SIAM, 1987.

[21] C. Sanderson and R. Curtin. Armadillo: a template-based c++ library for linear algebra. *Journal of Open Source Software*, 1:26, 2016.

[22] *Intel Math Kernel Library for Linux OS - Developer Guide*.

[23] M. J. Frisch, G. W. Trucks, H. B. Schlegel, G. E. Scuseria, M. A. Robb, J. R. Cheeseman, G. Scalmani, V. Barone, B. Mennucci, G. A. Petersson, H. Nakatsuji, M. Caricato, X. Li, H. P. Hratchian, A. F. Izmaylov, J. Bloino, G. Zheng, J. L. Sonnenberg, M. Hada, M. Ehara, K. Toyota, R. Fukuda, J. Hasegawa, M. Ishida, T. Nakajima, Y. Honda, O. Kitao, H. Nakai, T. Vreven, J. A. Montgomery, Jr., J. E. Peralta, F. Ogliaro, M. Bearpark, J. J. Heyd, E. Brothers, K. N. Kudin, V. N. Staroverov, R. Kobayashi, J. Normand, K. Raghavachari, A. Rendell, J. C. Burant, S. S. Iyengar, J. Tomasi, M. Cossi, N. Rega, J. M. Millam, M. Klene, J. E. Knox, J. B. Cross, V. Bakken, C. Adamo, J. Jaramillo, R. Gomperts, R. E. Stratmann, O. Yazyev, A. J. Austin, R. Cammi, C. Pomelli, J. W. Ochterski, R. L. Martin, K. Morokuma, V. G. Zakrzewski, G. A. Voth, P. Salvador, J. J. Dannenberg, S. Dapprich, A. D. Daniels, Ö. Farkas, J. B. Foresman, J. V. Ortiz, J. Cioslowski, and D. J. Fox. Gaussian-09 Revision D.01. Gaussian Inc. Wallingford CT 2009.

[24] J.B. Tennyson, F. Peter, L.R.Brown, A. Campargue, A.G. Császár, L. Daumont, R.R. Gamache, J.T. Hodges, O.V. Naumenko, O.L. Polyansky, L.S. Rothman, A.C. Vandaele, N.F. Zobov, A.R. Derzi, C. Fábri, A.Z. Fazliev, T. Furtenbacher, I.E. Gordon, L. Lodi, and I.I. Mizus. Iupac critical evaluation of the rotational–vibrational spectra of water vapor, part iii: Energy levels and transition wavenumbers for {H216O}. *jqsrae*, 117:29–58, 2013.

View Article Online
DOI: 10.1039/C6CP06698D

[25] J.B. Tennyson, F. Peter, L.R.Brown, A. Campargue, A.G. Császár, L. Daumont, R.R. Gamache, J.T. Hodges, O.V. Naumenko, O.L. Polyansky, L.S. Rothman, A.C. Vandaele, N.F. Zobov, N. Dénes, A.Z. Fazliev, T. Furtenbacher, I.E. Gordon, S. Hu, T. Szidarovsky and I.A. Vasilenko. Iupac critical evaluation of the rotational–vibrational spectra of water vapor, part IV: Energy levels and transition wavenumbers for {D216O}, {D217O} and {D218O}. *jqsrae*, 142:93–108, 2014.

[26] Jr. T.H. Dunning. Gaussian basis sets for use in correlated molecular calculations. i. the atoms boron through neon and hydrogen. *J. Chem. Phys.*, 90:1007, 1989.

[27] A. D. Becke. Density-functional thermochemistry. III. The role of exact exchange. *jcp*, 98:5648–5652, 1993.

[28] R. Krishnan, J. S. Binkley, R. Seeger, and J. A. Pople. Self-consistent molecular orbital methods. XX. A basis set for correlated wave functions. *jcp*, 72:650–654, 1980.

[29] R.A. Kendall, T.H. Dunning Jr., and R.J. Harrison. Electron affinities of the first row atoms revisited. systematic basis sets and wave functions. *J. Chem. Phys.*, 96:6796, 1992.

[30] G. D. Dickenson, M. L. Niu, E. J. Salumbides, J. Komasa, K. S. E. Eikema, K. Pachucki, and W. Ubachs. Fundamental vibration of molecular hydrogen. *Physical Reviews Letter*, 110:193601, 2013.

[31] H. Hamaguchi, I. Suzuki, and A. D. Buckingham. Determination of derivatives of the polarizability anisotropy in diatomic-molecules .1. theoretical considerations on vibration-rotation raman intensities. *Molecular Physics*, 43:963, 1981.

[32] D.W. Firth, K. Beyer, M.A. Dvorak, S.W. Reeve, A. Grushov, and K.R.Leopold. Tunable far-infrared spectroscopy of malonaldehyde. *J.Chem.Phys.*, 94:1812, 1991.

[33] H.A. Fry, L.H. Jones, and J.E. Barefield. Observation and analysis of fundamental bending mode of t2o. *Journal of Molecular Spectroscopy*, 103(1):41 – 55, 1984.

View Article Online
DOI: 10.1039/C6CP06698D

[34] S.D. Cope, D.K. Russell, H.A. Fry, L.H. Jones, and J.E. Barefield. Analysis of the fundamental asymmetric stretching mode of t2o. *Journal of Molecular Spectroscopy*, 120(2):311 – 316, 1986.

[35] Shi Shun-Ping, Zhang Quan, Zhang Li, Wang Rong, Zhu Zheng-He, Jiang Gang, and Fu Yi-Bei. Geometrical structures, vibrational frequencies, force constants and dissociation energies of isotopic water molecules (h 2 o, hdo, d 2 o, hto, dto, and t 2 o) under dipole electric field. *Chinese Physics B*, 20(6):063102, 2011.